https://doi.org/10.1142/9789811280184_0020

Chapter 20

The SND@LHC experiment

Giovanni De Lellis
University of Naples "Federico II", Physics Department,
via Cintia 19, 80126, Naples, Italy

1. Introduction

As the accelerator with the highest beam energy, the LHC is also the source of the most energetic human-made neutrinos. Indeed, the LHC produces an intense and strongly collimated beam of TeV-energy neutrinos along the direction of the proton beams. Notably, this neutrino beam includes a sizable fraction of tau neutrinos, mainly produced via the $D_s \to \tau\nu_\tau$ decay and subsequent τ decays, and hence provides a novel opportunity to study their properties.

Already in 1984, De Rujula and Rückl proposed to use the LHC neutrino beam by placing a neutrino experiment in the far forward direction.[1] This idea of detecting LHC neutrinos was revisited several times in the following decades.[2,3] More recently, a feasibility study was carried out, resulting in the estimate of the physics potential and in the identification of a proper location underground in the LHC tunnel for such an experiment to operate during the Run 3 of the LHC.[4,5] In 2018, the FASER collaboration installed a suitcase size pilot detector employing emulsion films and recently reported the first neutrino interaction candidates at the LHC.[6]

SND@LHC, Scattering and Neutrino Detector @ LHC, is a compact experiment designed to perform measurements with neutrinos produced at the LHC in the unexplored pseudo-rapidity region of $7.2 < \eta < 8.4$, complementary to all the other experiments at the LHC, including FASER.[7] The Collaboration submitted an LoI in August 2020[8] and a Technical Proposal in January 2021.[9] The experiment was approved in March 2021.

2. Experiment concept

The experiment is located 480 m downstream of IP1 in the TI18 tunnel, an injection tunnel during LEP operation. The detector consists of a hybrid system based on an 830 kg target mass of tungsten plates, interleaved with emulsion and electronic trackers, followed downstream by an hadronic calorimeter and a muon identification system, as shown in Fig. 1. The emulsion films with their micrometric accuracy[10] constitute the vertex detector while trackers in the target region, based on the Scintillating Fibre technology,[11] provide the time stamp to the events and complement emulsion for the electromagnetic energy reconstruction. Nuclear emulsion films are readout by state-of-the-art, fully automated, optical scanning systems.[12–15] The hadronic calorimeter and muon system comprises of eight layers of scintillating bar planes interleaved with 20 cm-thick iron slabs. The three most downstream stations are made of fine grained bars with both horizontal and vertical orientation (to trace the penetrating muons). Every scintillating bar as well as every fibre module is viewed by SiPMs.

The detector configuration allows efficient differentiation between all three neutrino flavours, as well as searching for Feebly Interacting Particles via signatures of scattering in the detector target.[16] The first phase aims at operating the detector throughout Run 3 to collect about 290 fb^{-1}.

The detector takes full advantage of the space available in the TI18 tunnel to cover the desired range in pseudo-rapidity. Figure 2 shows the top and side views of the detector positioned inside the tunnel. It is worth noting that the tunnel floor is sloped, as can be seen from the side view, with the floor sloping down along the longitudinal axis of the detector. As shown in the top view, the nominal collision axis from IP1 comes out of the

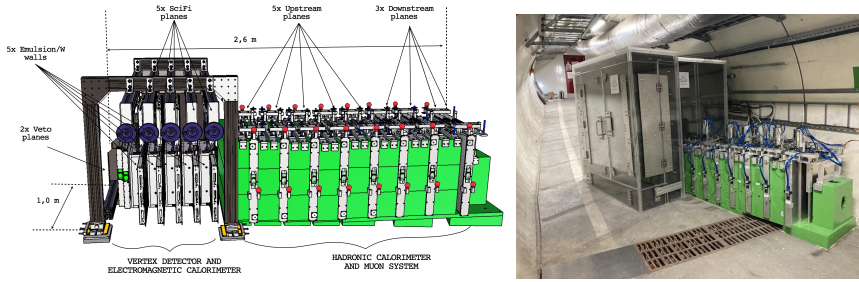

Fig. 1. Detector layout (left) and picture of the detector installed in TI18 (right).

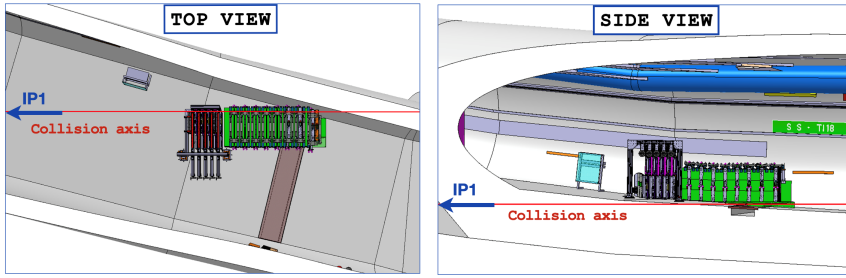

Fig. 2. Side and top views of the SND@LHC detector in the TI18 tunnel.[9]

floor very close to the wall of the tunnel. The location is ideal to explore the off-axis region.[17] Since no civil engineering work could have been done in time for the operation in Run 3, the tunnel geometry imposed several constraints. The following guidelines were adopted for the optimisation of the detector design: a good calorimetric measurement of the energy requires about 10 λ_{int}; a good muon identification efficiency requires enough material to absorb hadrons; for a given transverse size of the target region, the azimuthal angular acceptance decreases with the distance from the beam axis. The energy measurement and the muon identification set a constraint on the minimum length of the detector. With the constraints from the tunnel, this requirement competes with the azimuthal angular acceptance that determines the overall flux intercepted and therefore the total number of observed interactions. The combination of position and size of the proposed detector is an optimal compromise between these competing requirements. The geometrical constraints also restrict the detector to the first quadrant only around the nominal collision axis, as shown in the top view of the detector in Fig. 2.

The result is a compact detector, 2.6 m in length. The energy measurement and the muon identification limit the target region to a length of about 80 cm. The transverse size downstream of about 80(H) $\times$ 60(V) cm^2 is limited by the constraint of the tunnel side wall. The transverse size of the target region is proportionally smaller in order to match the acceptance of the energy measurement and the muon identification for the vertices identified in the target volume. In order to maximise the number of neutrino interactions, tungsten has been selected as the passive material. The emulsion target will be replaced a few times each year, during technical stops of the LHC.

With data from Run 3, SND@LHC will be able to study more than two thousand high-energy neutrino interactions.

All the detector systems were constructed in the labs by Summer 2021 and were assembled and tested at CERN. In October 2021, a test-beam was performed at the SPS with protons of different energies in order to calibrate the response of the hadronic calorimeter. Moreover, the full detector was commissioned on the surface at CERN with penetrating muons in the H6 experimental hall. On November 1st, the installation underground started. A borated polyethylene shielding box was added to surround the target and absorb low-energy neutrons originated from beam-gas interactions: its installation was completed by March 15^{th} 2022 as can be seen in the right picture of Fig. 1. The detector installation was completed on April 7^{th} 2022 by adding the target walls with emulsion films, and it is now taking data with the Run 3 of the LHC. The apparatus and its performance during the commissioning phase are extensively described in a dedicated paper.[18]

In the following sections we review the physics case of the experiment and the future prospects.

2.1. *QCD measurements*

Electron neutrinos in $7.2 < \eta < 8.4$ range are mostly produced by charm decays. Therefore, ν_es can be used as a probe of charm production in an angular range where the charm yield has a large uncertainty, to a large extent coming from the gluon parton distribution function (PDF). Electron neutrino measurements can thus constrain the uncertainty on the gluon PDF in the very small (below 10^{-5}) x region. The interest therein is two-fold: gluon PDF in this x domain will be relevant for Future Circular Collider (FCC) detectors; secondly, the measurement will reduce the uncertainty on the flux of very-high-energy atmospheric neutrinos produced in charm decays, essential for the evidence of neutrinos from astrophysical sources.[19,20] The charm measurement in Run 3 will be affected by a systematic uncertainty at the level of 30% and by a statistical uncertainty of 5%.

The left plot of Fig. 3 shows the ratio between charm measurements in different η regions normalised to the LHCb measurement:[21] gluon PDF uncertainty provides the largest contribution. SND@LHC will measure charm in the $7.2 < \eta < 8.4$ region where the PDF uncertainty is dominant.

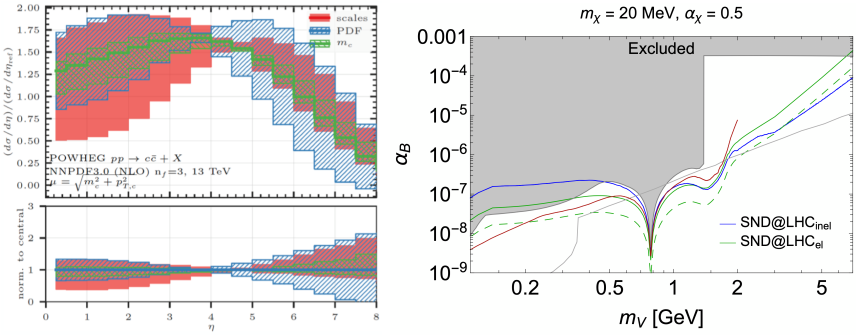

Fig. 3. Left: Ratio between the differential cross-section at 13 TeV and the differential cross-section at 7 TeV, with the latter evaluated in the pseudo-rapidity range $4 < \eta < 4.5$.[9] Right: Sensitivity of the SND@LHC experiment to the leptophobic portal[16]

2.2. *Lepton flavour universality with neutrino interactions*

In the pseudo-rapidity range of interest, tau neutrinos are essentially only produced in $D_s \to \tau\nu_\tau$ and the subsequent τ decays. One can thus assume that the source of both ν_e and ν_τ is essentially provided by semi-leptonic and fully leptonic decays of charmed hadrons. Unlike ν_τs produced only in D_s decays, ν_es are produced in the decay of all charmed hadrons, essentially: D^0, D, D_s, and Λ_c. Therefore, the ν_e/ν_τ ratio depends only on the charm hadronisation fractions and decay branching ratios. The systematic uncertainties due to the charm-quark production mechanism cancel out, and the ratio becomes sensitive to the ν-nucleon interaction cross-section ratio of the two neutrino species. The measurement of this ratio can thus be considered a lepton flavour universality test in neutrino interactions.

Charmed hadron fractions and ν branching ratios in the experiment acceptance produce a systematic uncertainty on this ratio of about 22% while the statistical uncertainty is dominated by the low statistics of the ν_τ sample, which corresponds to a 30% uncertainty.[9] The systematic uncertainty was evaluated by studying the fluctuations of the ratio using different event generators, after having equalised the branching ratio $D_s \to \tau\nu_\tau$ to the PDG value.[22]

Lepton flavour universality can also be tested with the electron to muon neutrino ratio. The ν_μs are much more abundant but heavily contaminated by π and K decays, and therefore the production mechanism cannot be considered the same as in the case of ν_e. However, this contamination is mostly concentrated at low energies. Above 600 GeV, the contamination is

predicted to be reduced to about 35%, and stable with the energy. Moreover, charmed hadron decays have practically equal branching ratios into electron and muon neutrinos. As a result, the ν_e/ν_μ ratio provides a test of the lepton flavour universality with an uncertainty of 15%, with an equal 10% statistical and systematic contribution.[9]

2.3. *Feebly Interacting Particles*

The experiment is also capable of performing model-independent direct searches for FIPs. They may be produced in the *pp* scattering at the LHC interaction point, propagate to the detector and decay or scatter inside it. The background from neutrino interactions can be rejected by a time-of-flight measurement.

A recent work[16] summarises the experiment's sensitivity to physics beyond the Standard Model, by considering the scatterings of light dark matter particles χ via leptophobic $U(1)_B$ mediator, as well as decays of Heavy Neutral Leptons, dark scalars and dark photons. The excellent spatial resolution of nuclear emulsions makes SND@LHC suited to search for neutral mediators decaying into two charged particles.

SND@LHC is unique in its capability to perform a direct dark matter search at accelerators. The right plot of Fig. 3 shows the sensitivity of the experiment to the leptophobic portal under the assumption that $m_\chi = 20$ MeV and the coupling of the mediator to χ particles is $\alpha_\chi = 0.5$. The considered signatures are the elastic scattering off protons (green line, 10 signal events) and the deep-inelastic scattering (blue line, 100 signal events). The dashed line corresponds to the upgraded setup that may operate during Run 4. The red line shows the 100 event contour for the DUNE experiment.[23]

2.4. *Future upgrade*

An advanced version of the SND@LHC detector is envisaged for the HL-LHC. It will consist of two detectors: the FAR detector placed in the same η region as SND@LHC and the NEAR detector in the region $4 < \eta < 5$. The FAR detector will perform the charm production measurement and lepton flavour universality tests with neutrinos at the percent level, and the NEAR detector will benefit from the overlap with LHCb to reduce systematic uncertainties and will perform neutrino cross-section measurements. In order to increase the azimuth angle coverage of the NEAR detector, a location in existing caverns, closer to the interaction point, will be searched for.

Each detector will be made of three elements. The upstream one is the target region for the vertex reconstruction and the electromagnetic energy measurement with a calorimetric approach. It will be followed downstream by a muon identification and hadronic calorimeter system. The third and most downstream element will be a magnet for the muon charge and momentum measurement, thus allowing for neutrino/anti-neutrino separation for ν_μ and for ν_τ in the muonic decay channel of the τ lepton.

The target will be made of thin sensitive layers interleaved with tungsten plates, for a total mass of a few tons. Given that the use of nuclear emulsion at the HL-LHC may be incompatible with technical stops, the Collaboration is investigating the use of compact electronic trackers with high spatial resolution fulfilling both tasks of vertex reconstruction with micrometric accuracy and electromagnetic energy measurement. The hadronic calorimeter and the muon identification system will also be optimised.

References

1. A. De Rujula and R. Ruckl, Neutrino and muon physics in the collider mode of future accelerators. In *SSC Workshop: Superconducting Super Collider Fixed Target Physics*, pp. 571–596 (5, 1984). doi: 10.5170/CERN-1984-010-V-2.571.
2. A. De Rujula, E. Fernandez, and J. Gomez-Cadenas, Neutrino fluxes at future hadron colliders, *Nucl. Phys. B.* **405**, 80–108 (1993). doi: 10.1016/0550-3213(93)90427-Q.
3. H. Park, The estimation of neutrino fluxes produced by proton-proton collisions at $\sqrt{s}$ = 14 TeV of the LHC, *JHEP.* **10**, 092 (2011). doi: 10.1007/JHEP10(2011)092.
4. S. Buontempo, G. M. Dallavalle, G. De Lellis, D. Lazic, and F. L. Navarria, CMS-XSEN: LHC Neutrinos at CMS. Experiment Feasibility Study (4, 2018).
5. N. Beni et al., Physics Potential of an Experiment using LHC Neutrinos, *J. Phys. G.* **46** (11), 115008 (2019). doi: 10.1088/1361-6471/ab3f7c.
6. H. Abreu et al., First neutrino interaction candidates at the lhc, *Phys. Rev. D.* **104**, L091101 (Nov, 2021). doi: 10.1103/PhysRevD.104.L091101. URL `https://link.aps.org/doi/10.1103/PhysRevD.104.L091101`.
7. H. Abreu et al., Detecting and Studying High-Energy Collider Neutrinos with FASER at the LHC, *Eur. Phys. J. C.* **80** (1), 61 (2020). doi: 10.1140/epjc/s10052-020-7631-5.
8. SND@LHC Collaboration. Scattering and Neutrino Detector at the LHC. Technical report, CERN, Geneva (Aug, 2020). URL `http://cds.cern.ch/record/2729015`.
9. C. Ahdida et al. SND@LHC - Scattering and Neutrino Detector at the LHC.

Technical report, CERN, Geneva (Jan, 2021). URL https://cds.cern.ch/record/2750060.
10. C. W. Fabjan and H. Schopper, eds., *Particle Physics Reference Library: Volume 2: Detectors for Particles and Radiation*. Springer Nature, Cham (2020). ISBN 978-3-030-35317-9, 978-3-030-35318-6. doi: 10.1007/978-3-030-35318-6.
11. LHCb Collaboration. LHCb Tracker Upgrade Technical Design Report. Technical report (Feb, 2014). URL http://cds.cern.ch/record/1647400.
12. A. Alexandrov et al., A new fast scanning system for the measurement of large angle tracks in nuclear emulsions, *JINST*. **10** (11), P11006 (2015). doi: 10.1088/1748-0221/10/11/P11006.
13. A. Alexandrov et al., A new generation scanning system for the high-speed analysis of nuclear emulsions, *JINST*. **11** (06), P06002 (2016). doi: 10.1088/1748-0221/11/06/P06002.
14. A. Alexandrov et al., The Continuous Motion Technique for a New Generation of Scanning Systems, *Sci. Rep.* **7** (1), 7310 (2017). doi: 10.1038/s41598-017-07869-3.
15. A. Alexandrov, G. De Lellis, and V. Tioukov, A Novel Optical Scanning Technique with an Inclined Focusing Plane, *Sci. Rep.* **9** (1), 2870 (2019). doi: 10.1038/s41598-019-39415-8.
16. A. Boyarsky, O. Mikulenko, M. Ovchynnikov, and L. Shchutska, Searches for new physics at SND@LHC, *JHEP*. **03**, 006 (2022). doi: 10.1007/JHEP03(2022)006.
17. N. Beni et al., Further studies on the physics potential of an experiment using LHC neutrinos, *J. Phys. G*. **47** (12), 125004 (2020). doi: 10.1088/1361-6471/aba7ad.
18. G. Acampora et al., SND@LHC: The Scattering and Neutrino Detector at the LHC, https://arxiv.org/pdf/2210.02784.pdf, to appear on JINST.
19. A. Bhattacharya et al., Prompt atmospheric neutrino fluxes: perturbative QCD models and nuclear effects, *JHEP*. **11**, 167 (2016). doi: 10.1007/JHEP11(2016)167.
20. Y. S. Jeong et al., Neutrinos from charm: forward production at the LHC and in the atmosphere, *PoS*. **ICRC2021**, 1218 (2021). doi: 10.22323/1.395.1218.
21. R. Aaij et al., Measurements of prompt charm production cross-sections in pp collisions at $\sqrt{s} = 13$ TeV, *JHEP*. **03**, 159 (2016). doi: 10.1007/JHEP03(2016)159. [Erratum: JHEP 09, 013 (2016), Erratum: JHEP 05, 074 (2017)].
22. PDG, P. A. Zyla et al., Review of Particle Physics, *PTEP*. **2020** (8) (08, 2020). ISSN 2050-3911. doi: 10.1093/ptep/ptaa104. URL https://doi.org/10.1093/ptep/ptaa104. 083C01.
23. S. Naaz, J. Singh, and R. B. Singh, DUNE prospect for leptophobic dark matter, *Advances in High Energy Physics*. **2020**, 1–9 (Nov, 2020). doi: 10.1155/2020/9047818. URL https://doi.org/10.1155%2F2020%2F9047818.